galaxies

IMPACT FACTOR 3.8

CITESCORE 6.3

Article

Single Parameter Model for Galaxy Rotation Curves

Sophia N. Cisneros, Rich Ott, Meagan Crowley, Amy Roberts and Marcus Paz

Special Issue

Alternative Interpretations of Observed Galactic Behaviors

Edited by

Prof. Dr. Anne M. Hofmeister and Prof. Robert E. Criss

MDPI

https://doi.org/10.3390/galaxies14010012

galaxies

MDPI

Article

Single Parameter Model for Galaxy Rotation Curves

Sophia N. Cisneros [1,*,†], Rich Ott [2,†], Meagan Crowley [3,†], Amy Roberts [4,†] and Marcus Paz [5,†]

[1] Department of Astronomy, University of Washington, 1410 NE Campus Pkwy, Seattle, WA 98195, USA
[2] Department of Physics, Massachusetts Institute of Technology, 77 Massachusetts Ave., Cambridge, MA 02139, USA; rott@alum.mit.edu
[3] Department of Chemistry, Colorado School of Mines, 1500 Illinois St., Golden, CO 80401, USA; mcrowley1@mines.edu
[4] Department of Physics, University of Colorado Denver, 1201 Larimer St., Denver, CO 80204, USA; amy.roberts@ucdenver.edu
[5] Department of Physics, University of Denver, 2199 S University Blvd., Denver, CO 80210, USA; marcus.paz@du.edu
* Correspondence: sofcis94@uw.edu
† These authors contributed equally to this work.

Abstract

One key piece of evidence for dark matter is the rotation-curve problem: the disagreement between measured galactic rotation curves and their luminous mass. A novel solution to this problem is presented here, in a model that predicts observed Doppler-shifted spectra based only on the luminous matter estimates and one free model parameter α. This model is applied to fit the rotation curves of the SPARC sample of 175 galaxies, yielding mass-to-light ratios, goodness of fit measurements, and α. The measured average $\chi^2_r = 2.24$ compares favorably with the Navarro-Frenk-White dark matter model's average of $\chi^2_r = 4.19$ for the same data, and more galaxies are successfully fit by this model. The model provides a useful formulation linking luminous matter to the observed rotation curves, with the dark matter contribution to galaxies encoded in two transformation terms of the luminous mass. It also offers a lower-parameter characterization of the rotation curve problem, and a power law relationship between α and galactic photometric quantities is observed, potentially removing the need for the free parameter.

Keywords: galaxy rotation curves; galaxy dark matter; Milky Way galaxy

Academic Editors: Anne M. Hofmeister, Anne M. Hofmeister and Robert E. Criss

Received: 22 November 2025
Revised: 10 February 2026
Accepted: 13 February 2026
Published: 15 February 2026

1. Introduction

At the level of the data, the rotation-curve problem in spiral galaxies arises from the discrepancy between velocities inferred from Doppler-shifted spectra and those derived from luminous mass observations [1–4]. Because both velocities serve as proxies for mass, this discrepancy has been a cornerstone for positing a missing mass component—dark matter. Despite extensive searches, both direct and indirect detection experiments have thus far yielded null results [5,6]. Following the Large Hadron Collider's null results for a dark matter candidate and as direct-detection experiments approach the ever-present neutrino background [7], it is imperative to systematically explore alternative explanations for rotation curve phenomenology.

NEW—Historically, Ostriker and Peebles [8] and Rubin et al. [9] treated the dark matter problem in spiral galaxies as a distinct physics problem from the cosmological context. In this work, we follow that convention, focusing exclusively on the rotation-curve problem. This choice is motivated by compelling correlations between luminous

and dark matter in this context [3,4,10,11], which lack a clear physical basis [2,10,12–16]. The Universal Rotation Curve (URC), discovered by Persic et al. [17] and Salucci and Burkert [18], shows that when 1100 galaxy rotation curves are normalized by their scale lengths and plotted together, they naturally fall into three groups: flat rotation curves at the median, large galaxy rotation curves inflecting downwards, and small galaxy rotation curves inflecting upwards. Notably, the Milky Way lies at the median of this distribution. Since there is no a priori reason for the Milky Way to occupy this position, we interpret this as hinting at frame-dependent effects associated with the Milky Way.

The dark matter paradigm interprets the URC phenomenology that galaxies larger than the Milky Way have minimal dark matter halos, while galaxies smaller than the Milky Way are dark matter dominated. This interpretation is less than satisfactory, because it contradicts classical gravity on which dark matter theories are built. Classical gravity requires that mass accretion rates are directly proportional to the initial mass function [19]. Accordingly, we take this as motivation to characterize dark matter phenomenology in this context through frame effects associated with the Milky Way, while remaining agnostic about its underlying physics. This approach yields a simpler rotation curve formula with only one free parameter, compared to at least two in NFW and Einasto dark matter models [20], and successfully fits a greater number of galaxies. Case studies demonstrating the flexibility of this model across all three classes of rotation curves are provided in Appendix B.

The necessity of reducing the parameter space is directly connected to the study of luminous mass modeling in spiral galaxies. Luminous mass modeling is a tricky business, precisely because the Doppler-shifted spectra observations—expected to constrain such models—instead introduced the dark matter problem and at least two more free parameters [21]. Luminous mass models, which underpin rotation curve formulae, already include three parameters to scale the luminous mass components of a spiral galaxy: stellar disk, stellar bulge, and gas halo. Embedded in these three scaling parameters there is a cascade of model-dependent parameter choices [22]. The process of stellar population synthesis modeling, which frames a galaxy's mass budget, relies on matching the photometric measurement of a galaxy's spectral energy density (SED) to a suite of under-constrained parameters [23]. To extract a meaningful model for a given SED, assumptions must be made regarding the history of star formation and evolution, stellar metallicities and abundances, the states and quantities of gas and dust, dust attenuation and extinction—and this is by no means an exhaustive list [24]. Currently no single model can encompass the full range of the parameter space for galaxies, so models are stitched together, with poorly constrained physics assumptions [25–27]. The SDSS IV MaSTAR Stellar Spectral Library [28] has significantly increased coverage and standardization in the field, and yet the theoretical modeling of galaxy SEDs remains a convolution of all these effects—making disentanglement difficult and resulting in large uncertainties in the resulting luminous mass model [29].

The approach presented here offers a promising avenue to refine modeling techniques and constrain galaxy mass estimates. This model does not alter classical physics, but encodes gravitational effects in galaxy frames using standard relativistic tools applied in a novel context. We note that previous studies which have ruled out general relativity in this context [30] did not compare relative galaxy frames as *ratios* of galaxy gravitational potentials, one-to-one in radii, as we do. We use the resulting model to fit the 175 well-studied spiral galaxy rotation curves in the SPARC sample [29] and show how this model's free parameter appears to be highly correlated to a ratio of photometric quantities.

Other models, including Newtonian mass approaches and geometric analyses of galaxies [31–33], do not appear as tightly constrained as the present approach. Modified Newtonian Dynamics (MOND) Milgrom [34] remains a notable alternative, effectively

reproducing rotation curves, but represents a modification of classical gravitational physics rather than a re-expression of frame-dependent effects. In Section 4.4 we describe some of the other models which have been employed in the spiral galaxy rotation problem, in comparison to our model.

The paper is organized as follows: Section 2 describes the transition from the standard dark matter rotation curve formula to this paper's form; Section 3 details the methods used to fit spiral galaxy rotation curve data using our model; Section 4 summarizes the key results; and Section 5 presents conclusions and future perspectives. Detailed galaxy data, tables of fit results compared to dark matter models, and selected figures are presented in Appendix A, while individual galaxy case studies are highlighted in Appendix B.

2. Rotation Curve Fitting Models

2.1. Dark Matter Rotation Curve Formula

The standard rotation curve (RC) formula

$$v(r)_{dyn}^2 = v(r)_{lum}^2 + v(r)_{dm}^2 \tag{1}$$

gives the dark matter model prediction $v(r)_{dyn}$, which is fitted to the rotation curve velocity parameter $v(r)_{obs}$ which is a kinematic representation of the observed Doppler-shifted spectra from a Lorentz boost. Terms in $v(r)_{lum}$ represent the orbital velocities due to the luminous mass, interpreted by classical Poisson gravity. Terms in $v(r)_{dm}$ represent the orbital velocities due to the dark matter halo.

2.2. Relative-Frame Rotation Curve Formula

We construct our model's rotation curve formula by representing the standard dark matter contribution in Equation (1) via a convolution of frame effects parameterized solely by luminous mass estimates. All transformations are defined one-to-one in radius between the observed galaxy and the host galaxy. Our modified rotation curve formula is then

$$v(r)_{rc}^2 = v(r)_{lum}^2 + \alpha\kappa(r)^2 S(r)_1 S(r)_2, \tag{2}$$

for $v(r)_{rc}$ the model's prediction which is fitted to the rotation curve velocity parameter $v(r)_{obs}$. We maintain the physical meaning of the terms $v(r)_{lum}$ as representative of the physical orbital motion due to the luminous mass. We assume luminosity to be Lorentz scalar under a reliable distance indicator and therefore invariant to the relativistic transformations of 4-vectors below. We note the SPARC sample spans a distance range of 0.97 to 125.65 Mpc. The term α is the model's free fitting parameter.

Terms in $\kappa(r)$ are ratios of the Newtonian gravitational potentials from luminous mass estimates

$$\kappa(r) = \frac{\Phi(r)_{gal}}{\Phi(r)_{mw}} \tag{3}$$

for the galaxy being observed $\Phi(r)_{gal}$, by that of the Milky Way $\Phi(r)_{mw}$. Then terms $S(r)_1$ are defined by the transformation

$$S(r)_1 = \sinh\zeta(r), \tag{4}$$

for the pseudo-rapidity ζ defined by

$$e^{\zeta(r)} = \sqrt{\frac{(1-2\Phi(r)_{gal})}{(1-2\Phi(r)_{mw})}}, \tag{5}$$

https://doi.org/10.3390/galaxies14010012

which represent the curved 2-frame mapping between the galaxies, where all terms are ratios of the Schwarzschild clock terms in the weak field limit. Equivalently, terms can be seen as ratios of the norms of the timelike Killing fields, which are invariants of the spacetime [35].

To use the Cartan frame-field technique, one is required to transform the curved 2-frame back to the flat tangent frames where observations are made. We accomplish that transformation with

$$S(r)_2 = \cosh \tau(r) \tag{6}$$

for the pseudo-rapidity τ defined by the sum of the pseudo-rapidity for the curved 2-frame transformation in Equation (5) and the pseudo-rapidity for the flat frame-fields η,

$$e^{\tau(r)} = e^{(\zeta(r)+\eta(r))}. \tag{7}$$

Terms in $e^{\eta(r)}$ return the transformations to the flat frame-fields

$$e^{\eta(r)} = \sqrt{\frac{1+\beta(r)}{1-\beta(r)}} \tag{8}$$

as they are defined by the Keplerian velocity due to the luminous mass $\beta(r) = v(r)_{lum}/c$, and are therefore our best approximation of the flat frame-fields. This assumption is validated by the fact that dark matter is not required to reproduce the rotation curve of our solar system.

We emphasize that all terms on the right-hand side of our rotation curve formula, Equation (2), are now parameterized solely in terms of luminous mass and a single free parameter, α. Graphical representations of the two transformations are provided in Figure 1. While our model is framed in the spirit of the Cartan field frames [36], we remain agnostic regarding the underlying physics of dark matter, and instead present a compact reformulation of the dark matter contribution that achieves good fits with fewer free parameters. This heuristic treatment leverages the separability of effects on the frequency of light due to relative translational motion versus acceleration of the source [37], as well as the symmetry of the rotation curve data [17].

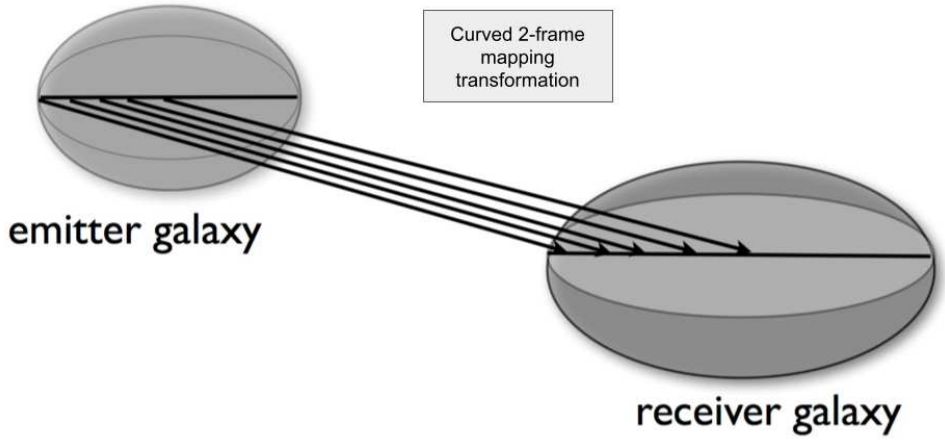

(**a**)

Figure 1. *Cont.*

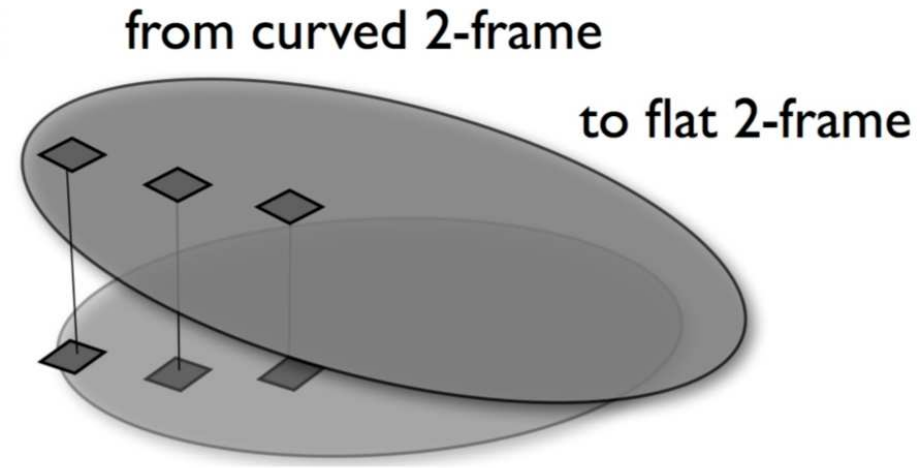

(**b**)

Figure 1. Graphical Representations of Our Transformations (**a**) Curved 2-frame transformation $S(r)_1$ and (**b**) curved-to-flat transformation $S(r)_2$.

Additionally, since Lorentz-type transformations are strictly applicable to inertial frames, we note Rindler [38]'s observation that to compare galaxies as inertial frames is to compare them from their respective centers. In Section 3.2, we demonstrate a suitable choice of boundary conditions for calculating the gravitational potentials, ensuring that galaxies are compared consistently from their respective centers.

3. Methods

3.1. Luminous Mass Modeling

The baryonic mass components of a spiral galaxy are represented kinematically by $v(r)^2_{disk}$ for the stellar disk, $v(r)^2_{bulge}$ for the stellar bulge, and $v(r)^2_{gas}$ for the gas halo,

$$v(r)^2_{lum} = \gamma_b v(r)^2_{bulge} + \gamma_d v(r)^2_{disk} + v(r)^2_{gas}. \tag{9}$$

Terms in $v(r)_{lum}$ represent the total expected circular orbital velocities about the galactic rotation axis due to the luminous mass. Terms in γ_b and γ_d are mass-to-light ratios which come from the complex process of modeling the luminous mass associated with a given spectral energy density as described in Section 1. Contributions from the gas $v(r)_{gas}$ are calculated from a different observational technique [39], and do not require mass-to-light ratios.

The only inputs to our model are the Newtonian mass models published kinematically in the SPARC database at https://astroweb.case.edu/SPARC/MassModels_Lelli2016c.mrt accessed on 10 January 2026 which come from the best photometry currently available. Detailed descriptions of the photometry and mass models are given in Appendix A.

3.2. Gravitational Potential

Classically the Newtonian gravitational potential $\Phi(r)$ is calculated by the integral

$$\Phi(r) = -\int_{r_1}^{r_2} \vec{F} \cdot \vec{dr}, \tag{10}$$

for $\vec{F}$ the central gravitational force and $\vec{dr}$ the path of the integration from an initial value of $\Phi(r)_{lum} = 0$ at $r_1 \to \infty$ to a negative maxima $\Phi(r)_{total}$, at the small limit $r_2 \to 0$. In practice this integration begins at the largest observed radius $r_1 = R_{max}$ and is summed into a negative maxima at the smallest observed radius $r_2 = r_{min}$. This classical boundary

condition is an implicit assumption of an asymptotically flat embedding space, where the total energy goes to zero at infinity. However the complexity of streamlines in the cosmic web [40] demonstrate that asymptotic flat space has not been recovered at the large R limit of observed galaxies.

Motivated by the astute observation of Rindler [38], that to compare galaxies inertially is to compare them from their respective centers, we flip the bounds of integration such that all galaxies are compared from a common zero at $r \approx 0$ and summed to a positive definite value which approaches a constant for most galaxies. While the central black holes of galaxies do not have a mass of zero, their mass is vanishingly small with respect to the mass of the galaxy disk and bulge.

Gravitational potentials calculated in this way satisfy the Poisson equation and populate Schwarzschild clock terms $g(r)_{tt} = -(1 - 2\Phi(r))$. Since what we measure in practice is the difference in potentials, this technique allows galaxies to be compared inertially so that we can use Lorentz-type transformations in Equations (4) and (6), while maintaining contact with the classical usages of the potential.

3.3. Geometric Simplifications

The Luminous mass modeling problem for spiral galaxies (see Equation (9)) usually assumes spherical symmetry for the stellar bulge and gas halo, but axial symmetry for the stellar disk [41–44]. However, it is a common technique to use spherical symmetry for the entire mass distribution as proof of concept [45–48]. Numerical integration of the thin stellar disk is computationally intensive, requiring extra assumptions of under-constrained boundary conditions and relevant physical scales [49]. For these reasons we have used the spherically symmetric approximation and the Schwarzschild metric in this work.

Gravitational potentials calculated for a spherical symmetry versus a thin disk geometry converge to the same value at lengths greater than one-third of the galaxy's exponential scale-length R_e [50]. Since this is the region where dark matter effects become important [4], this calculational technique is justified. However in the inner region of a galaxy, where our gravitational potential integrations begin, the spherical assumption overestimates the gravitational potential by a factor of ≈2. This factor of 2 can be clearly seen in our average fit results for the disk mass-to-light ratios in Tables A2 and A3. Implementation of an exponential disk geometry would resolve this artifact of the analysis, but at significant computational expense [51].

3.4. Fitting Procedure

A Python program was developed to fit galaxy rotation curve data using our model, and is publicly available at https://github.com/Cisneros-Galaxy/RCFM accessed on 10 January 2026. The fitting procedure is as follows: first, a Milky Way baryon model is selected. Appendix A.2 compares the two Milky Way (MW) models used successively in this work. The MW model data in $v(r)_{lum}$ is read into the program for a series of measurements in radii. The galactic gravitational potential is then calculated by numerically integrating as in Section 3.2. Once the MW potential is calculated, it remains static for the rest of the fitting procedure.

Data for the galaxies being observed include several pieces of information: the RC velocities $v(r)_{obs}$ from Doppler-shifted spectra, the uncertainty on that measurement $v(r)_{err}$, and the components of the luminous mass represented kinematically by $v(r)_{bulge}$, $v(r)_{disk}$, and $v(r)_{gas}$ as in Section 3.1. To calculate the baryonic potential for the galaxy in question, $v(r)_{lum}$ is first computed as per Equation (9), with the starting values for the mass-to-light ratios of the bulge and disk respectively set at $\gamma_b = 1$ and $\gamma_d = 1$. Mass to light ratios are

described in Section 3.1. The $\Phi(r)_{gal}$ associated with the galaxy is then computed as in Section 3.2.

After the potentials due to the luminous mass of the galaxy being studied and the MW are calculated, the components must be compared at matching values of r. To match radii, $\Phi(r)_{mw}$ is interpolated to produce values at the radii reported in the observed galaxy RC data $v(r)_{obs}$. Any galaxy observations with radii larger than the largest radius in the MW model are discarded.

The model's parameter α is set to its starting value, and the model prediction is then assembled to give $v(r)_{rc}$ as in Equation (2), which is fitted to the galaxy's RC data $v(r)_{obs}$. The parameters α, γ_b and γ_d are allowed to freely vary, recomputing $\Phi(r)_{gal}$ and $v(r)_{rc}$ at each step, and optimal values are determined by the minimization of the χ^2. The `scipy.optimize.curve_fit` utility in Python is used to perform this minimization. This fit is repeated for several different starting values of α (powers of 10 from 10^{-3} to 10^2) and the best fit is kept. We fit the 175 galaxies in the SPARC database [29], described in detail in Appendix A.

3.5. Number of Free Parameters

We present the model in this paper as a single-parameter framework. Here, we disregard the mass-to-light ratio parameters for the stellar disk and bulge, since the rotation curve fitting models we compare against (both dark matter and MONDian models) include these parameters in common. Dark matter models typically require between 2 and 9 free parameters, while MOND models require two, in addition to the stellar mass-to-light ratios. Since the mass-to-light ratios are shared across dark matter and MOND models [34,52,53], we treat them as observational constraints from photometry and population synthesis modeling rather than as "free" parameters.

The under-constrained nature of luminous mass modeling arises because Doppler-shifted spectra, expected to constrain photometric measurements and population synthesis modeling, instead introduce additional free parameters in the context of dark matter halos. A class of models known as Forward Newtonian models, which predict baryonic mass densities directly from Doppler-shifted spectra, are not compared to this work; while these models represent a long-term goal, current formulations do not directly constrain luminous mass modeling.

With this accounting, dark matter models have a minimum of two free parameters [54], MONDian models have a minimum of two [55], and the present model has one. Furthermore, as shown in Section 4.2, the model's free parameter appears highly correlated with a ratio of photometric quantities—luminosity and half-light radius—suggesting the possibility of a zero-parameter representation of dark matter phenomenology purely in terms of luminous mass estimates.

4. Results

4.1. Goodness of Fits

Rotation curve fitting models can be compared using two metrics obtained from the fitting procedure: the reduced χ^2_r values and the mass-to-light ratios. Since error estimates on rotation curve (RC) velocities have not been standardized across the field [56,57], average χ^2_r values can only be meaningfully compared when fitted to the same RC data.

We fit the 175 galaxy RCs in the SPARC database [29], which have previously been analyzed with the Navarro-Frenk-White (NFW) dark matter model (using λCDM priors) from Li et al. [21]. In the standard dark matter approach, the gravitational contributions from stars and gas are estimated, and the cold dark matter halo is parametrically modeled to predict the rotation curve velocity, which is then fitted to the observed Doppler-shifted

velocities. For the entire SPARC sample, the NFW model has an average $\chi_r^2 = 4.19$, while our model, using the Xue-Sofue-Jiao MW parameters [58–60], has an average $\chi_r^2 = 2.25$, and with the McGaugh-Jiao MW [60,61], the average $\chi_r^2 = 4.36$.

For the SPARC sample, the NFW dark matter model average mass-to-light ratios are $\gamma_{disk} = 0.51$ and $\gamma_{bulge} = 0.62$. For our model using the Xue-Sofue-Jiao MW, the averages are $\gamma_{disk} = 1.11$ and $\gamma_{bulge} = 0.77$, while for the McGaugh-Jiao MW, they are $\gamma_{disk} = 1.02$ and $\gamma_{bulge} = 0.68$. As expected, our disk mass-to-light ratios are approximately a factor of 2 larger than those from the NFW model due to the use of a standard spherical approximation for the galactic disk, which reduces computational complexity and minimizes excess parameters. As noted by Chatterjee [50], the spherical approximation overestimates γ_{disk} by a factor of $\approx$2 at radii less than $R/3$, which is where our fits set the zero for the sums of the galaxy potentials. This implies that the true disk mass-to-light ratio for our model is closer to $\gamma_{disk} \approx 0.5$–$0.6$. These values are consistent with reported errors on luminous mass estimates of $\pm$20% [62], and future developments will employ a full thin-disk geometry to improve accuracy.

Taken together, these metrics indicate that our model provides a compact reformulation of the rotation curve fitting problem: it achieves comparable or better fits than the NFW model while using fewer free parameters. Individual galaxy results are reported in Table A2, for our model with respect to the Xue-Sofue-Jiao MW alongside the NFW model for comparison.

4.2. Free-Parameter Correlation

To frame a more reliable comparison, we select a subset of SPARC galaxies with the highest quality data based on the following criteria:

1. Galaxies with the most accurate distance estimates (Tip of the Red Giant Branch [63] and Cepheid variable stars [64]), rejecting all others.
2. Galaxies with sky inclinations between 15° and 80°, excluding those with inclinations greater than 80°, where surface brightness profiles are uncertain, and less than 15°, where line-of-sight Doppler shifts are unreliable.
3. Excluding galaxies with a quality factor $Q = 3$, which are not suited for dynamical studies. The SPARC database [29] assigns $Q = 1$ for high-quality rotation curves, $Q = 2$ for minor asymmetries or lower-quality curves, and $Q = 3$ for major asymmetries, strong non-circular motions, or offsets between HI and stellar distributions.

This selection results in a subset of 36 galaxies, reported in Table A3, representing the highest-quality rotation curves and photometric models with well-established distances. All galaxies are local (<15 Mpc) and undisturbed, which minimizes distance-related selection biases and includes a variety of dwarf, gas-dominated galaxies.

For this subset, the NFW dark matter model has an average $\chi_r^2 = 5.46$ and fails to fit two galaxies (NGC6789 and UGC07232). Our model fits all galaxies, yielding an average $\chi_r^2 = 1.64$ for the Xue-Sofue-Jiao MW [58–60] and $\chi_r^2 = 1.65$ for the McGaugh-Jiao MW [60,61].

The two MW models differ primarily in central concentration: the Xue-Sofue-Jiao MW has a de Vaucouleurs stellar bulge, whereas the McGaugh-Jiao MW has a more diffuse bulge-bar structure. Our model, tested on the full SPARC sample, slightly prefers the Xue-Sofue-Jiao MW, but for the high-quality subset, both MW models yield remarkably low χ_r^2 values, providing confidence in the model's consistency with the SPARC rotation curve data. At this level, there is no strong distinguishing feature between MW models.

To explore the physical interpretation of the model's free parameter, α (Equation (2)), we plot the ratio of total luminosity L to half-light radius R from an auxiliary file in the SPARC database [29] versus the fitted α for each galaxy in the subset. Here, L is in units of

$10^9 L_\odot$ and R in kpc, both measured in the 3.6 μm band with a solar absolute magnitude of 3.24 [65]. The resulting distributions are well fit by power laws (Figure 2):

For the Xue-Sofue-Jiao MW, we find the α parameter form is

$$\alpha = 93.2\left(\frac{L}{R}\right)^{-1.11} \tag{11}$$

with a coefficient of determination of $R^2 = 0.82$. For the McGaugh-Jiao MW, we find the α parameter form is

$$\alpha = 35\left(\frac{L}{R}\right)^{-0.953} \tag{12}$$

with a coefficient of determination of $R^2 = 0.72$. These power-law fits are shown in Figure 2.

Since all other terms in Equation (2) are ratios of galaxy quantities relative to the Milky Way, and α is dimensionless, we propose that α may itself be expressed as a ratio of L/R terms:

$$\alpha = \left(\frac{(L/R)_{mw}}{(L/R)_{gal}}\right)^b \tag{13}$$

Using the coefficients from Equations (11) and (12), this correlation function predicts a MW luminosity given its half-light radius. For the Xue-Sofue-Jiao MW, this yields $L_{MW} = 0.89 \times 10^9 L_\odot$ with $R = 0.5$ kpc; for the McGaugh-Jiao MW, $L_{MW} = 6.85 \times 10^9 L_\odot$ with $R = 4.2$ kpc. As we are embedded in the Milky Way, it is difficult to determine which estimate is more physically realistic, though upcoming surveys such as the Vera C. Rubin Observatory's LSST [66] will continue to refine constraints on the Milky Way's structure and mass content.

Taken together, the strong correlation between α and photometric quantities suggests that, for high-quality data, the model's single free parameter may be largely predictable from luminous mass estimates alone. In other words, this provides a methodological pathway toward a zero-parameter representation of rotation curve fits, without making claims about the existence or absence of dark matter.

4.3. Comparing Milky Way Models

The model presented in this paper requires a static background choice for the Milky Way (MW) baryon distribution. Determining the gravitational potential of the MW from our position inside the disk is notoriously difficult [67,68], and the galaxy's baryon distribution remains an active area of research. Previous studies [20] suggest that a substantial dark matter component is required, while Jeans equation analyses indicate that long-term dynamical stability of a disk necessitates a large shell of concentric matter [8,48]. More recent analyses of GAIA DR3 data [69] suggest that the MW may require only a minimal dark matter halo, and Jiao, Yongjun et al. [60] indicate that the MW rotation curve is approximately Keplerian out to at least 26.5 kpc.

Regardless of the outcome of this debate, our goal is not to weigh in on the existence of MW dark matter halos. Instead, we introduce a simple, novel reformulation of the contribution commonly attributed to dark matter. By encoding these effects as frame-field transformations parameterized by luminous mass estimates, the problem becomes more tractable, with only a single free parameter.

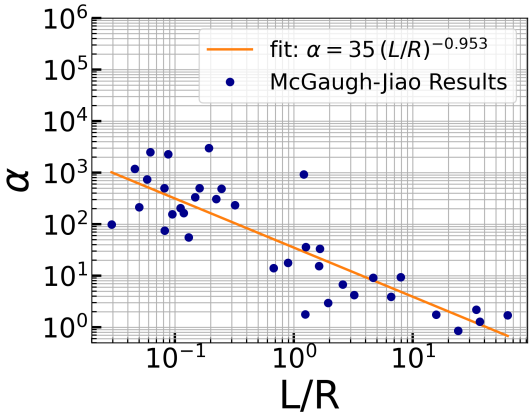

(**a**)

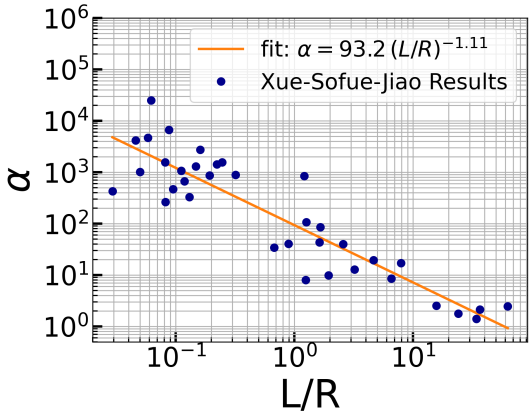

(**b**)

Figure 2. Physical Interpretation of the Model's free parameter $\alpha \propto L/R$. For L the total luminosity in units of $10^9 M_\odot$ and R the half-light radius in units of kpc. There is one α value per galaxy in the subset of the most reliable SPARC galaxy data described in Table A3 and Section 4. We report results with respect to the MW baryon model from (**a**) McGaugh-Jiao and (**b**) Xue-Sofue-Jiao.

Due to ongoing uncertainties regarding the MW, we have chosen two widely used MW baryon models to fit the SPARC galaxy sample. A detailed summary of these two MW models is provided in Appendix A.2, and a comparison of the results is given in Table A3. The main distinction between the models lies in their central mass concentration and the framework used to extend the rotation curves due to the baryons.

The MW model from Xue-Sofue [58,70] has a highly concentrated central mass, represented by a de Vaucouleurs-law stellar bulge with a half-mass scale radius of 0.5 kpc. It is modeled using the NFW dark matter framework combined with Jeans Equation analysis informed by SDSS observations of 2400 blue horizontal branch stars.

The MW model from McGaugh [61] has a more diffuse triaxial bulge-bar with a scale length of 4.2 kpc. It is modeled using the MOND-RAR framework and Jeans Equation analysis informed by GAIA and APOGEE data. Based on average χ^2_r values, our model slightly favors the centrally condensed Xue-Sofue MW over the McGaugh MW. However, for the subset of galaxies with the most reliable data, the two MW models produce virtually indistinguishable fits. In future work, we plan to extend our analysis to all 56 MW baryon models from Lin and Li [71], exploring the impact of different bulge, disk, and gas halo assumptions on high-quality rotation curves.

Residuals for each MW model were computed by subtracting the model-predicted velocities from the observed SPARC rotation velocities at each radius. Figure 3 shows

the distributions of these normalized residuals for all 175 galaxies and both MW models. In all cases, the residuals are narrowly centered around zero with a range of approximately ± 3 standard deviations, though with some heavy tails. Their similar behavior across MW models indicates that our fitting parameters are robust to the choice of MW baryon distribution.

Gaussian fits to the residual distributions, obtained using `scipy.curve_fit` function in Python, yield the following: for the McGaugh-Jiao MW model, mean $= 0.023$ and standard deviation $= 0.744$; for the Xue-Sofue-Jiao MW model, mean $= -0.020$ and standard deviation $= 0.824$ (all in units of standard deviations in velocity error). The small values associated with these quantities in both cases provide confidence that our fits match data closely.

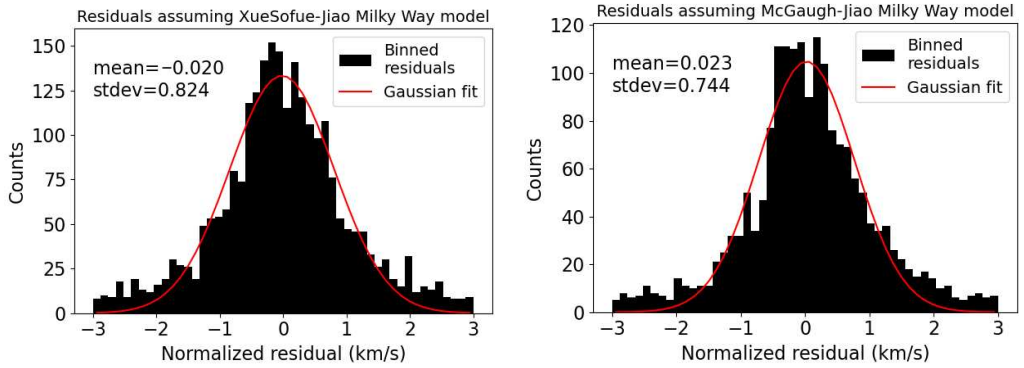

(**a**) (**b**)

Figure 3. Normalized residuals for fits to SPARC galaxies assuming two different MW baseline models, each fitted by a Gaussian function. The means and standard deviations of the Gaussian fit are shown. (**a**) For the Xue-Sofue-Jiao Milky Way (**b**) For the McGaugh-Jiao Milky Way.

4.4. Comparisons to Other Alternative Formulations of the Rotation Curve Problem

Alternative approaches have been proposed to explain the observed linkages between luminous and dark matter in galaxies. The most widely known is Modified Newtonian Dynamics (MOND) [34], which modifies classical gravity by introducing a characteristic acceleration scale a_0. MOND and the Radial Acceleration Relation (RAR) have been applied to all SPARC galaxies, yielding average χ^2 values comparable to NFW dark matter fits. Both MOND and dark matter models assume that Doppler-shifted spectra directly reflect the rotation velocities.

Another class of model are the Newtonian orbital models (NOMs) which rely solely on luminous mass without modifying gravity. Examples include Sipols and Pavlovich [32] and Feng [33], which solve the inverse problem of inferring baryonic mass directly from rotation curves. While promising as zero-parameter models, NOMs achieve full consistency with photometry in only $\sim$62% of galaxies; the remainder require additional low-luminosity mass components.

Other alternative efforts look at geometry and the characterization of the gravitational potential, such as Hofmeister and Criss [31], who analyze the problem using oblate spheroid spin rather than thin-disk approximations. As discussed in Section 3.2, the thin-disk gravitational potential differs from that of a spherical mass distribution at both small radius, where a disk-like geometry requires more mass for a given acceleration, and at large radii where less mass is required [50]. So, by characterization of the oblate spheroid shape of real galaxies and spin, instead of simply a thin-disk, Hofmeister and Criss [31] find a model which requires only 4/9 of the baryonic mass predicted by NOMs. Another interesting approach from Feng [33] introduces a "galactic rotation parameter" A to account for

deviations from spherical symmetry, with A ranging from 1 to 2. However, some predicted densities, particularly for the MW, exceed observational constraints [72]. These studies provide interesting insights into the problem, but are difficult to compare directly to our model due to the framing of our results in terms of reduced χ^2 and mass-to-light ratios.

Relativistic formulations, including TeVeS [45] and the metric-skew-tensor model [73], reproduce MOND successes for galaxy rotation curves without non-baryonic dark matter. TeVeS introduces vector and scalar fields to modify gravity but suffers from nonphysical caustic instabilities at high energies. Brownstein's approach fits ∼100 galaxies but does not report χ^2 or mass-to-light ratios, making direct comparison difficult. Importantly, both modify classical gravity, whereas our model retains standard relativistic physics and instead encodes dark matter-like effects through Cartan frame-field transformations of the host galaxy.

In summary, while MOND, NOMs, and relativistic modifications provide valuable insights, they either modify fundamental physics or remain incomplete. In contrast, our model fits all 175 SPARC galaxies with a single free parameter, using only luminous mass estimates and standard relativistic principles.

5. Conclusions

The early view of dark matter was that the galactic [2] and cosmological [74–76] problems were distinct. We follow that precedent here, focusing exclusively on the rotation-curve problem. The model presented in this paper encodes the dark matter contribution in the standard rotation curve problem as a product of two relative galaxy frame transformations, parameterized solely by estimates of the luminous mass and a single free parameter. This result is then compared to dark matter models that typically employ at least two free parameters.

These transformations are constructed in the spirit of the Cartan frame-fields, where all terms are ratios of the timelike Killing fields between the galaxy being observed and the Milky Way observing frame. We avoid interpreting the physics of this approach with respect to the debate over the existence of dark matter, and instead simply demonstrate that encoding dark matter effects in terms of luminous mass provides excellent fits to a large sample of high-quality rotation curves. Independent of the physical interpretation of this model, it represents a one-parameter fit to rotation curve data, parameterized solely by estimates of the luminous mass, and constructed to reproduce the standard dark matter contribution to rotation curves.

We test our model on a sample of 175 high-quality rotation curves of spiral galaxies from the SPARC database [29] previously fitted by a NFW dark matter model, with λCDM priors, from Li et al. [21]. For the SPARC sample, our model with the Xue-Sofue-Jiao Milky Way results in an average reduced $\chi^2_r = 2.24$, whereas the NFW dark matter model gives an average reduced $\chi^2_r = 4.19$.

This approach re-purposes traditional physics transformations, to compare galaxies one-to-one in radius, but does not modify physics. Early investigations into the use of relativity to resolve the galaxy rotation curve problem used Galilean subtraction of the potentials at large radii [77], versus frame-field transformations appropriate to the four-vector algebra of Doppler-shifted frequencies. In addition, we show how a possible physical interpretation of the model's free parameter in terms of L/R, luminosity and effective radius, may be possible. Interpreting our model's free-parameter with a ratio of two photometric quantities could lead to a zero parameter model and a direct constraint to luminous mass modeling from the orthogonal observation of Doppler-shifted spectra. The upcoming observations from the Vera C. Rubin Observatory's Legacy Survey of Space and Time [66] will better inform the future Milky Way model used in this work.

https://doi.org/10.3390/galaxies14010012

Author Contributions: The work in this paper was divided as follow; conceptualization was by S.N.C.; methodology was by S.N.C., R.O. and A.R.; software, by R.O., A.R., M.C. and M.P.; validation, by R.O. and A.R.; formal analysis was by S.N.C., M.C., R.O., A.R. and M.P.; investigation was by S.N.C., M.C. and M.P.; data curation was S.N.C., M.C., R.O., A.R. and M.P.; writing—original draft preparation was by S.N.C.; writing—review and editing was by R.O., A.R. and M.C.; visualization was by R.O., M.C. and M.P.; and supervision was by S.N.C. All authors have read and agreed to the published version of the manuscript.

Funding: This research received no external funding.

Data Availability Statement: The code used to generate all figures and fit results is publicly available at https://github.com/Cisneros-Galaxy/RCFM, accessed on 22 October 2025. The rotation curve data and photometric models used in this paper are from the SPARC database publicly available at http://astroweb.cwru.edu/SPARC/, accessed on 22 October 2025. The few additional datasets included for comparison are available at the cited references.

Acknowledgments: This work is dedicated to Emmett Till. We acknowledge and express gratitude to the first nations peoples for their generosity, on whose unceded lands this was written; including but not limited to the the Coos, Lower Umpqua and Siuslaw Indians of Oregon, the Coast Salish bands of the Puget Sound, the Cheyenne and Arapaho Tribes and Ute Tribes of Colorado, the Navajo Nation and Pueblos of New Mexico, and the Algonquian and Iroquoian Peoples of Massachusetts and New York. The authors would like to thank V. P. Nair, T. Boyer, M. Kaku, I. Chavel, R. Walterbos, N. P. Vogt, S. McGaugh, A. Klypin, T. Quinn, S. Tuttle, M. Juric, R. Rivera, N.S. Oblath, J. Formaggio, J. Conrad, P. Fisher, Y. Sofue, C. Mihos, and M. Merrifield for their guidance. We wish to also thank the many students who have contributed to this work over the years, including but not limited to; A. Ashley, D. Battaglia, D. Chester, R. Robinson, A. Rodriguez, Z. Brown, P. Pham, Z. Holland, A. Livingston, L. Castrellon, R. Real Rico, E. Gutierrez-Gutierrez, S.J. Rubin, S. Graham, and L. Joyal. Finally, we sincerely thank the reviewers and the editor for their time and careful attention, which greatly improved the clarity and overall quality of the manuscript.

Conflicts of Interest: The authors declare no conflicts of interest.

Abbreviations

The following abbreviations are used in this manuscript:

RC	Rotation Curve
MW	Milky Way
SPARC	Spitzer Photometry and Accurate Rotation Curves
URC	Universal Rotation Curve
SED	Spectral Energy Density
SDSS	Sloan Digital Sky Survey
λCDM	λ Cold Dark Matter
RAR	Radial Acceleration Relation
NFW	Navarro-Frenk-White
NOMs	Newtonian orbital models
TeVeS	Tensor-Vector-Scalar

Appendix A. Figures, Tables and Detailed Information on Data Used

Appendix A.1. SPARC Database

We fit the Spitzer Photometry and Accurate Rotation Curves (SPARC) dataset of 175 nearby late type galaxies with the model presented in this paper. The SPARC sample provides extended RC data from atomic hydrogen (HI) and H-α [29]. HI provides the most reliable RCs because it is dynamically cold, traces circular orbits, and can be observed several effective radii past the stellar disk. This sample of rotationally supported galaxies spans the widest range of masses and morphologies presently available.

These galaxies are reported with Newtonian luminous mass models, represented kinematically as in Equation (9). These baryon mass distributions are based on Spitzer Photometry in the near infrared at 3.6 μm. Near infrared is believed to be the best tracer of stellar mass [78], as at this wavelength mass-to-light (γ_i) ratios are believed to be almost constant and independent of star formation history [78,79]. The SPARC database reports mass-to-light ratios set to $\gamma_i = 1$ in units of $M_\odot/L_\odot$ at 3.6 μm for all galaxies.

SPARC gas fractions are reported as $v(r)_{gas}$, calculated from surface density profiles of HI with the formalism given in [39] and scaled by a factor 1.33 to account for cosmological helium abundances. The addition of molecular gas could increase mass fractions in the inner kiloparsec of a galaxy [14], but are not included as most galaxies in the SPARC sample do not have molecular measurements available.

Error on these velocities is estimated at ±20% [29]. The SPARC database can be found at http://astroweb.cwru.edu/SPARC/, accessed on 22 October 2025.

Appendix A.2. Milky Way Luminous Mass Models

Our model requires a static choice of a MW luminous mass model to fit our observations of external galaxies. In this paper, we compare the SPARC sample of 175 galaxies successively to two different MW baryon models.

The MW model from McGaugh [61] has a triaxial bulge-bar in the center of the luminous mass distribution and the extended rotation curve comes from Radial Acceleration Relation (RAR) [80], a phenomenological model arising from analysis of Modified Newtonian Dynamics [34]. The MW from Sofue and Xue [58,59] has a de Vaucouleurs bulge and is extended by NFW dark matter modeling [81]. The difference between the two MW models is marked in the inner 7 kpc; as the McGaugh MW has a scale-length of 4.2 kpc and the Xue-Sofue MW model has a scale-length of 0.5 kpc. The Sofue model covers a range of 0 to 20 kpc, and the Xue MW model from 20 to 60 kpc. The Sofue and Xue MW models are from the same data and dark matter model extension, so are combined to increase coverage.

The recent ESA *Gaia* data release (DR3), [60] demonstrates a Keplerian decline of the rotation curve of the MW in the range of 9.5 to 26.5 kpc, consistent with our model. The ESA *Gaia* mission, taking measurements from the second Lagrange point, has revolutionized the science of the MW with unprecedented detail, statistical accuracy, and a drastic reduction in systematic uncertainties. Since this is the both the most recent and best data for the MW, we replace both models' MW velocities in the range from 9.5 to 26.5 kpc with those from [60]. We then shift the two sides of the given MW model by a constant amount to match the endpoints of the Jiao rotation curve. Hence, the Xue-Sofue MW model becomes the Xue-Sofue-Jiao MW and the McGaugh MW becomes the McGaugh-Jiao MW. See Table A1 for summary details.

Table A1. Milky Way Models. *NOTE:* The table lists the original model sources and assumptions. For both Milky Way models, we have replaced the original velocity data in the region spanning 9.5–26.5 kpc with the Gaia DR3 velocities reported by Jiao, Yongjun et al. [60] due to the high quality of the observations. Throughout the paper, these modified models are referred to as Sofue–Xue–Jiao and McGaugh–Jiao.

Author	Scale Length Bulge/Bar	Model for Extended RC	Range
Sofue-Xue [58,59]	0.5 kpc bulge	NFW dark matter [81]	[0, 60] kpc
McGaugh [61]	4.2 kpc bulge-bar	RAR [80]	[0, 150] kpc

Appendix A.3. Fit Results for the 175 SPARC Galaxies

This paper's model results in Table A2 are reported with respect to the Xue–Sofue–Jiao Milky Way model [58,60,70], because it performs significantly better than the McGaugh-Jiao Milky Way for the whole sample—though the two Milky Way models perform equally well on a more reliable subset of the SPARC galaxies. Table A3 reports our results for the subset for both Milky Way models, the McGaugh-Jiao and the Xue-Sofue-Jiao. Stellar mass-to-light ratios, γ_i, are given in units of solar mass per solar luminosity ($M_\odot/L_\odot$). Galaxies for which dark matter model fits fail are indicated by NaN.

Table A2. Fit Results for the SPARC 175 galaxy sample. Luminous models which did not include bulge components as reported in the SPARC database of Newtonian mass models are indicated by three dots.

Name	NFW Dark Matter			Our Model with XSJ MW			
	χ^2_r	γ_{disk}	γ_{bulge}	χ^2_r	γ_{disk}	γ_{bulge}	α
CamB	7.92	0.35	…	0.23	0.00	…	24,989.21
D512-2	NaN	NaN	NaN	0.21	1.48	…	131.01
D564-8	6.7	0.45	…	0.11	1.21	…	4130.26
D631-7	12.21	0.39	…	0.30	0.26	…	2725.54
DDO064	1.05	0.5	…	0.45	1.58	…	345.48
DDO154	16.57	0.33	…	10.58	1.18	…	1567.39
DDO161	1.99	0.47	…	0.62	0.97	…	279.60
DDO168	23.93	0.56	…	4.36	0.76	…	1290.43
DDO170	4.44	0.5	…	3.19	1.84	…	122.03
ESO079-G014	4.9	0.57	…	3.86	1.09	…	8.46
ESO116-G012	3.82	0.39	…	1.03	1.04	…	58.84
ESO444-G084	4.71	0.52	…	0.40	1.86	…	465.01
ESO563-G021	19.23	0.96	…	16.41	1.00	…	1.78
F561-1	1.21	0.49	…	1.05	0.96	…	0.00
F563-1	1.47	0.54	…	0.95	2.06	…	60.28
F563-V1	2.21	0.47	…	0.29	0.99	…	0.00
F563-V2	1.98	0.55	…	0.11	2.20	…	11.90
F565-V2	3.6	0.54	…	0.31	2.22	…	218.59
F567-2	NaN	NaN	NaN	0.50	1.31	…	29.40
F568-1	1.57	0.56	…	0.72	1.91	…	27.98
F568-3	4.99	0.55	…	1.79	1.31	…	68.81
F568-V1	0.31	0.53	…	0.14	2.14	…	9.17
F571-8	9.6	0.2	…	2.04	0.17	…	12,596.96
F571-V1	1.39	0.5	…	0.20	1.49	…	102.53
F574-1	2.21	0.54	…	1.42	1.54	…	20.27
F574-2	NaN	NaN	NaN	0.14	0.67	…	147.79
F579-V1	0.91	0.47	…	1.07	1.63	…	0.00
F583-1	2.23	0.59	…	1.04	1.87	…	128.01
F583-4	0.34	0.49	…	0.28	1.30	…	60.22
IC2574	36.3	0.44	…	2.27	1.10	…	885.47
IC4202	20.56	0.67	0.14	12.18	0.00	0.44	150.83
KK98-251	3.61	0.53	…	0.42	1.67	…	536.07
NGC0024	0.66	1.18	…	0.73	1.39	…	9.88
NGC0055	4.35	0.36	…	2.86	1.01	…	106.90
NGC0100	1.94	0.46	…	0.10	0.93	…	161.92
NGC0247	2.03	0.66	…	2.18	1.53	…	8.03

Table A2. *Cont.*

Name	NFW Dark Matter			Our Model with XSJ MW			
	χ_r^2	γ_{disk}	γ_{bulge}	χ_r^2	γ_{disk}	γ_{bulge}	α
NGC0289	2.06	0.53	…	1.78	0.74	…	3.59
NGC0300	0.93	0.41	…	0.42	1.14	…	85.28
NGC0801	7.15	0.72	…	7.38	0.77	…	0.82
NGC0891	4.39	0.25	0.54	1.89	0.66	0.00	3.46
NGC1003	2.54	0.66	…	3.42	0.77	…	80.54
NGC1090	2.77	0.54	…	2.27	0.81	…	4.88
NGC1705	1.33	0.82	…	0.13	1.25	…	35.94
NGC2366	3.91	0.31	…	2.34	1.06	…	446.13
NGC2403	9.09	0.39	…	10.73	0.86	…	19.32
NGC2683	2.66	0.66	0.67	1.01	0.88	0.44	1.78
NGC2841	1.47	1	0.88	1.36	0.91	1.10	1.40
NGC2903	6.54	0.27	…	7.45	0.62	…	2.62
NGC2915	1.05	0.44	…	0.63	0.56	…	841.91
NGC2955	4.27	0.32	0.82	4.45	0.40	0.88	1.80
NGC2976	1.45	0.6	…	0.46	0.91	…	40.19
NGC2998	3.53	0.55	…	3.74	0.87	…	2.14
NGC3109	15.31	0.92	…	0.28	2.05	…	661.98
NGC3198	1.46	0.46	…	1.72	0.88	…	8.51
NGC3521	0.29	0.5	…	0.77	0.71	…	1.67
NGC3726	3.27	0.49	…	2.41	0.76	…	8.32
NGC3741	1.74	0.55	…	0.65	0.71	…	6628.19
NGC3769	1.06	0.41	…	0.71	0.71	…	16.99
NGC3877	6.44	0.32	…	9.07	0.87	…	0.00
NGC3893	1.74	0.46	…	0.57	0.73	…	4.80
NGC3917	4	0.76	…	2.70	1.14	…	7.20
NGC3949	1.38	0.46	…	0.76	0.73	…	6.28
NGC3953	2.96	0.62	…	0.76	0.90	…	0.41
NGC3972	2.94	0.55	…	2.08	1.03	…	17.63
NGC3992	1.58	0.56	…	1.68	1.04	…	1.88
NGC4010	4.56	0.46	…	1.90	0.85	…	38.02
NGC4013	0.95	0.54	0.82	1.53	0.54	1.43	6.04
NGC4051	3.53	0.47	…	1.91	0.81	…	0.98
NGC4068	10.89	0.44	…	0.27	0.80	…	1383.44
NGC4085	15.12	0.39	…	2.83	0.58	…	44.82
NGC4088	0.66	0.39	…	0.87	0.63	…	4.78
NGC4100	1.29	0.57	…	1.90	0.95	…	3.50
NGC4138	7.83	0.62	0.7	0.75	0.98	0.00	1.98
NGC4157	0.57	0.48	0.67	0.61	0.69	0.56	4.08
NGC4183	0.33	0.46	…	0.53	1.24	…	9.51
NGC4214	1.01	0.54	…	1.19	1.01	…	42.96
NGC4217	3.27	0.98	0.22	1.33	1.13	0.46	6.24
NGC4389	26.19	0.32	…	0.20	0.31	…	562.73
NGC4559	0.3	0.43	…	0.34	0.77	…	18.47
NGC5005	0.09	0.5	0.55	0.07	0.62	0.69	1.36
NGC5033	3.44	0.35	0.39	6.39	0.85	0.52	1.36
NGC5055	2.54	0.26	…	6.29	0.62	…	2.12
NGC5371	5.03	0.26	…	12.55	0.78	…	0.49
NGC5585	6.94	0.21	…	6.35	0.75	…	149.12
NGC5907	5.52	0.3	…	7.88	0.94	…	2.27

Table A2. *Cont.*

Name	NFW Dark Matter			Our Model with XSJ MW			
	χ_r^2	γ_{disk}	γ_{bulge}	χ_r^2	γ_{disk}	γ_{bulge}	α
NGC5985	2.38	0.28	0.65	3.84	0.00	1.98	13.73
NGC6015	8.89	0.55	…	13.06	0.99	…	4.41
NGC6195	2.06	0.36	0.84	2.95	0.41	0.81	1.73
NGC6503	1.58	0.41	…	1.44	0.75	…	16.96
NGC6674	3.42	1.29	0.92	3.98	0.70	1.87	0.68
NGC6789	NaN	NaN	NaN	0.57	1.41	…	865.65
NGC6946	1.7	0.5	0.53	1.75	0.64	0.58	2.52
NGC7331	0.81	0.42	0.61	1.05	0.53	1.17	2.46
NGC7793	0.94	0.55	…	0.75	0.89	…	12.82
NGC7814	0.7	0.65	0.57	0.63	0.38	0.68	1.70
PGC51017	22.6	0.44	…	2.31	0.80	…	0.00
UGC00128	3.71	0.53	…	6.16	1.64	…	14.71
UGC00191	6.09	0.58	…	2.45	1.38	…	35.72
UGC00634	NaN	NaN	NaN	5.83	1.57	…	73.92
UGC00731	0.54	0.55	…	0.08	3.79	…	26.23
UGC00891	NaN	NaN	NaN	1.45	1.34	…	545.08
UGC01230	1.7	0.52	…	0.80	1.71	…	7.96
UGC01281	1.88	0.55	…	0.34	1.42	…	587.19
UGC02023	NaN	NaN	NaN	0.06	0.72	…	1265.61
UGC02259	2.44	0.43	…	4.66	1.81	…	16.62
UGC02455	10.42	0.34	…	0.90	0.28	…	843.15
UGC02487	5.26	0.7	0.59	4.18	1.24	0.77	0.91
UGC02885	1	0.42	1.05	2.14	0.50	0.98	1.83
UGC02916	11.4	0.5	0.5	11.36	1.41	0.71	0.28
UGC02953	5.64	0.54	0.57	5.69	0.74	0.78	0.92
UGC03205	3.54	0.68	1.04	2.99	0.68	1.07	1.58
UGC03546	1.03	0.59	0.47	1.14	0.61	0.60	1.41
UGC03580	2.36	0.68	0.28	2.20	0.48	0.41	71.41
UGC04278	3.19	0.48	…	0.92	1.00	…	642.15
UGC04305	2.22	0.53	…	1.80	0.88	…	0.00
UGC04325	6.66	0.49	…	3.72	1.87	…	0.00
UGC04483	1.33	0.48	…	0.52	1.28	…	1016.96
UGC04499	1.84	0.47	…	1.54	1.14	…	94.39
UGC05005	1.38	0.49	…	0.09	1.03	…	164.00
UGC05253	2.5	0.28	0.75	5.65	0.53	0.72	1.37
UGC05414	10.59	0.47	…	0.19	1.06	…	218.15
UGC05716	2.49	0.45	…	3.81	1.52	…	148.84
UGC05721	1.37	0.47	…	0.84	1.11	…	79.50
UGC05750	2.08	0.52	…	0.47	1.57	…	39.99
UGC05764	10.91	0.45	…	9.45	3.70	…	49.28
UGC05829	0.6	0.51	…	0.07	1.85	…	145.88
UGC05918	0.31	0.51	…	0.21	2.31	…	12.08
UGC05986	7.1	0.49	…	1.69	1.15	…	39.53
UGC05999	NaN	NaN	NaN	3.56	1.27	…	128.32
UGC06399	1.75	0.56	…	0.22	1.43	…	53.24
UGC06446	0.36	0.51	…	0.17	1.69	…	48.05
UGC06614	0.28	0.47	0.71	1.20	0.72	0.59	7.81
UGC06628	0.9	0.51	…	0.57	0.83	…	0.00
UGC06667	3.46	0.64	…	2.41	3.77	…	0.00
UGC06786	0.87	0.4	0.61	0.69	0.50	0.66	6.56
UGC06787	18.57	1.1	0.3	24.78	0.73	0.57	2.24
UGC06818	9.52	0.41	…	1.24	0.53	…	2418.29
UGC06917	1.5	0.51	…	1.09	1.12	…	39.19

Table A2. *Cont.*

Name	NFW Dark Matter			Our Model with XSJ MW			
	χ_r^2	γ_{disk}	γ_{bulge}	χ_r^2	γ_{disk}	γ_{bulge}	α
UGC06923	4.67	0.47	…	0.88	0.80	…	124.98
UGC06930	0.54	0.5	…	0.55	1.25	…	13.66
UGC06973	3.82	0.21	0.48	0.41	0.36	0.81	12.97
UGC06983	0.77	0.54	…	0.77	1.26	…	28.24
UGC07089	1.22	0.46	…	0.15	0.95	…	132.60
UGC07125	0.76	0.49	…	1.18	1.08	…	55.91
UGC07151	3.73	0.72	…	1.30	1.15	…	32.08
UGC07232	NaN	NaN	NaN	0.76	0.82	…	1563.21
UGC07261	0.87	0.52	…	1.46	1.22	…	40.71
UGC07323	2.63	0.49	…	0.26	0.97	…	86.65
UGC07399	1.99	0.54	…	1.00	1.54	…	70.39
UGC07524	0.97	0.5	…	1.48	1.59	…	34.22
UGC07559	1.97	0.43	…	0.21	0.97	…	1061.77
UGC07577	3.11	0.37	…	0.06	0.67	…	4668.25
UGC07603	2.36	0.46	…	0.52	1.07	…	288.77
UGC07608	1.94	0.51	…	0.30	2.02	…	428.16
UGC07690	3.5	0.67	…	0.40	1.05	…	29.31
UGC07866	0.3	0.46	…	0.07	1.26	…	330.26
UGC08286	3.02	0.62	…	2.66	1.66	…	36.50
UGC08490	0.29	0.48	…	0.15	1.26	…	40.48
UGC08550	1.53	0.6	…	0.70	1.35	…	171.01
UGC08699	0.72	0.74	0.59	0.95	0.55	0.76	1.94
UGC08837	10.79	0.38	…	0.69	0.78	…	1422.40
UGC09037	2.13	0.25	…	1.55	0.58	…	26.53
UGC09133	7.17	0.75	0.53	7.50	0.77	0.72	0.71
UGC09992	NaN	NaN	NaN	0.04	1.30	…	0.10
UGC10310	1.63	0.51	…	0.12	1.54	…	19.21
UGC11455	5.47	0.61	…	3.98	0.76	…	2.41
UGC11557	2.06	0.47	…	0.91	0.60	…	73.80
UGC11820	2.63	0.58	…	1.44	1.24	…	145.34
UGC11914	0.87	0.34	0.91	1.61	0.04	0.89	2.46
UGC12506	0.26	0.43	…	1.18	1.35	…	1.20
UGC12632	0.45	0.48	…	0.21	1.86	…	31.86
UGC12732	0.26	0.5	…	0.18	1.51	…	82.38
UGCA281	1.46	0.5	…	0.28	1.23	…	339.55
UGCA442	7.38	0.61	…	0.86	2.28	…	261.55
UGCA444	0.23	0.51	…	0.10	3.78	…	425.75

Table A3. Best-fit Parameters for the most reliable SPARC Galaxy Data. *Column 2* Galaxies for which the dark matter model fails to find a fit are indicated by NaN. *Columns 3 & 4* Our model results with MW baseline from McGaugh-Jiao [60,61] indicated by **MJ**. *Columns 5 & 6* Our model results with MW baseline from from Xue-Sofue-Jiao [58–60] indicated by **XSJ**. *Columns 7 & 8* The reported distances and the total luminosity L in units of $10^9 M_\odot$ by the half-light radius R in units of kpc, as reported in the SPARC database [29].

Name	Dark Matter NFW	Our Model MJ		Our Model XSJ		Distance	L/R
	χ_r^2	χ_r^2	α	χ_r^2	α	(Mpc)	
CamB	7.92	0.81	2505.76	0.23	24,989.21	3.36	0.06
D564-8	6.70	0.03	1177.28	0.11	4130.26	8.79	0.05
D631-7	12.21	1.22	501.02	0.30	2725.54	7.72	0.16

Table A3. *Cont.*

Name	Dark Matter NFW χ^2_r	Our Model MJ χ^2_r	Our Model MJ α	Our Model XSJ χ^2_r	Our Model XSJ α	Distance (Mpc)	L/R
DDO154	16.57	6.15	500.74	10.58	1567.39	4.04	0.08
DDO168	23.93	4.55	330.48	4.36	1290.43	4.25	0.15
ESO444-G084	4.71	1.19	156.01	0.40	465.01	4.83	0.09
IC2574	36.30	1.69	233.95	2.27	885.47	3.91	0.32
NGC0024	0.66	0.94	2.96	0.73	9.88	7.30	1.93
NGC0055	4.35	1.51	35.98	2.86	106.90	2.11	1.26
NGC0247	2.03	2.36	1.78	2.18	8.03	3.70	1.25
NGC0300	0.93	0.44	33.21	0.42	85.28	2.08	1.65
NGC2403	9.09	14.13	9.06	10.73	19.32	3.16	4.65
NGC2683	2.66	0.96	0.85	1.01	1.78	9.81	24.08
NGC2841	1.47	1.19	2.20	1.36	1.40	14.10	34.14
NGC2915	1.05	0.59	917.03	0.63	841.91	4.06	1.21
NGC2976	1.45	0.47	6.77	0.46	40.19	3.58	2.57
NGC3109	15.31	0.35	164.55	0.28	661.98	1.33	0.12
NGC3198	1.46	1.31	3.88	1.72	8.51	13.80	6.55
NGC3741	1.74	0.60	2271.94	0.65	6628.19	3.21	0.09
NGC4214	1.01	1.60	15.38	1.19	42.96	2.87	1.63
NGC5055	2.54	7.70	1.28	6.29	2.12	9.90	36.58
NGC6503	1.58	1.72	9.31	1.44	16.96	6.26	7.93
NGC6789	NaN	0.08	2993.97	0.57	865.65	3.52	0.19
NGC6946	1.70	2.52	1.74	1.75	2.52	5.52	15.76
NGC7331	0.81	1.04	1.70	1.05	2.46	14.70	62.81
NGC7793	0.94	0.71	4.21	0.75	12.82	3.61	3.22
UGC04483	1.33	0.45	214.19	0.52	1016.96	3.34	0.05
UGC07232	NaN	0.85	488.75	0.76	1563.21	2.83	0.25
UGC07524	0.97	1.28	14.09	1.48	34.22	4.74	0.67
UGC07559	1.97	0.17	203.80	0.21	1061.77	4.97	0.11
UGC07577	3.11	0.06	737.74	0.06	4668.25	2.59	0.06
UGC07866	0.30	0.08	55.68	0.07	330.26	4.57	0.13
UGC08490	0.29	0.26	17.67	0.15	40.48	4.65	0.89
UGC08837	10.79	0.61	309.13	0.69	1422.40	7.21	0.22
UGCA442	7.38	0.72	74.81	0.86	261.55	4.35	0.08
UGCA444	0.23	0.12	98.80	0.10	425.75	0.98	0.03

Appendix B. Individual Galaxy Comparisons

In this appendix we highlight the Universal Rotation Curve Spectrum groupings [10] the three classes of rotation curves; declining, flat and ascending.

Appendix B.1. Declining Rotation Curves

As can be seen in Figure A1, our model provides excellent fits to the well studied, high-surface brightness, spiral galaxies NGC 2841, NGC 5055, and NGC 3521. Wiegart [82] has noted that these are galaxies with declining rotation curves that are not well explained by the usual dark matter morphology scenarios. The under-constrained nature of luminous mass modeling [23] is highlighted for NGC 5055, with a luminous mass model from Lelli et al. [29], Battaglia et al. [83] with no central stellar bulge, and one from de Blok et al. [56] which does.

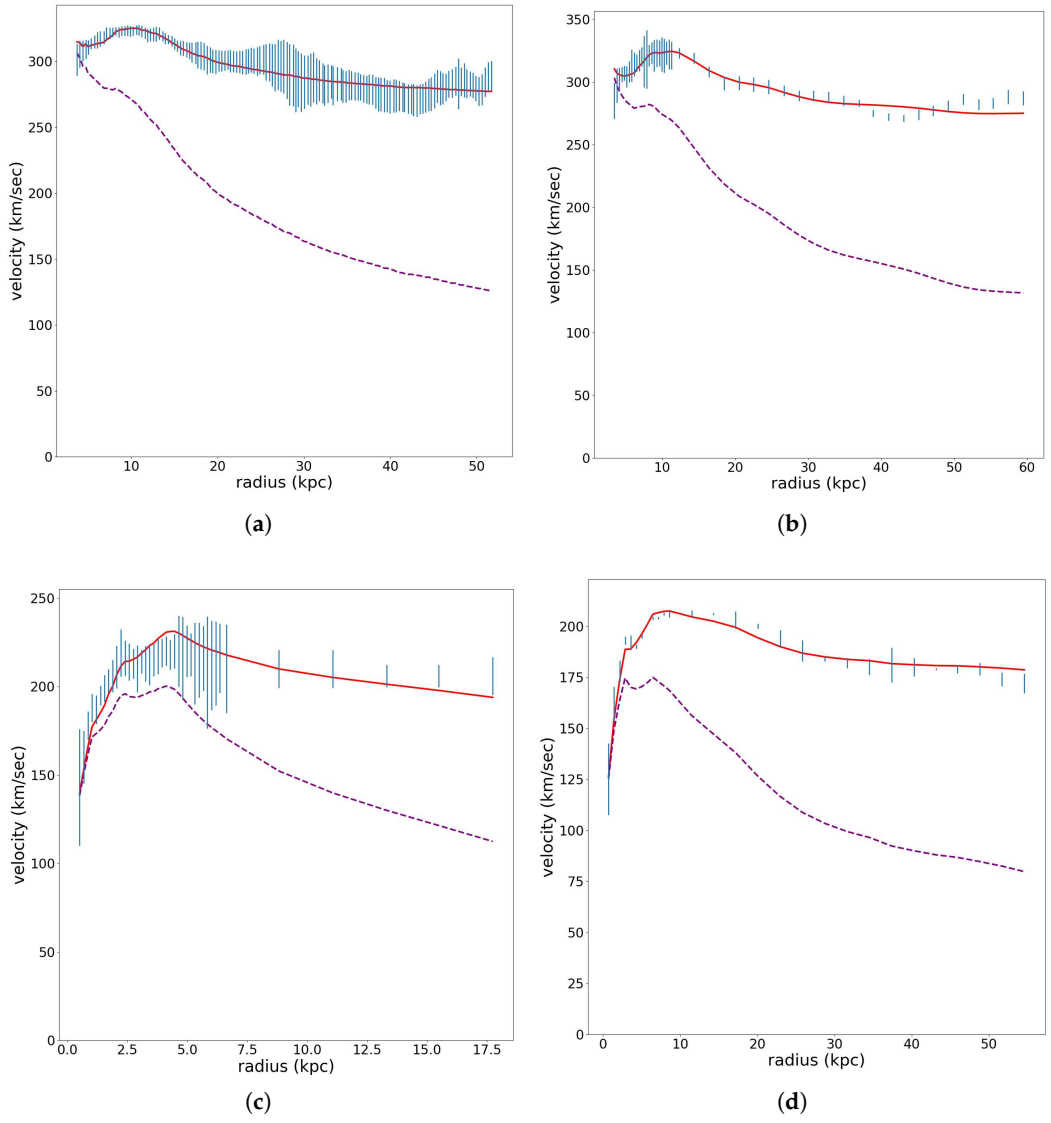

Figure A1. *Cont.*

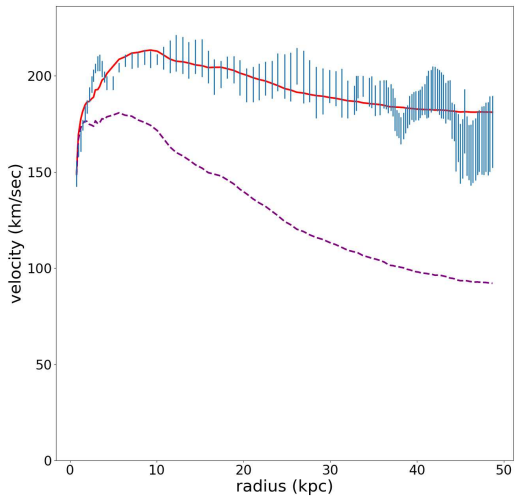

(**e**)

Figure A1. Declining Rotation Curves of high-surface brightness galaxies. Rotation curve data (blue points with error bars) and the input baryonic mass model (purple dashed line). This model's fits are shown by the red solid line, with respect to the Xue-Sofue-Jiao Milky Way. (**a**) NGC 2841 [56], (**b**) NGC 2841 [29], (**c**) NGC 3521 [29], (**d**) NGC 5055 [29], (**e**) NGC 5055 [56].

Appendix B.2. Truly Flat Rotation Curves

As can be seen in Figure A2, our model provides excellent fits to galaxies with truly flat rotation curves. We include NGC 3198, whose rotation curve is truly flat in comparison to NGC 891 and NGC 7814, whose rotation curves inflect about flat. NGC 3198 is a barred spiral in Ursa Major, which has no bulge component. The spiral galaxies NGC 7814 and NGC 891 present an interesting test case to dark matter models, because both galaxies are presented edge-on on the sky and have essentially identical RCs, but extreme opposite luminous mass morphologies. NGC 7814 is bulge dominated and NGC 891 is an almost entirely disk galaxy. In [84] the question is raised, "why are these RCs so identical if their dark matter halos are necessarily different to accommodate the differences in the luminous mass?" In the paradigm of this paper's model the two RCs are very similar in magnitude, but differ in their inflections at large radii. In fact, it is such a subtle difference that it particularly highlights the power of this framing of the rotation curve problem.

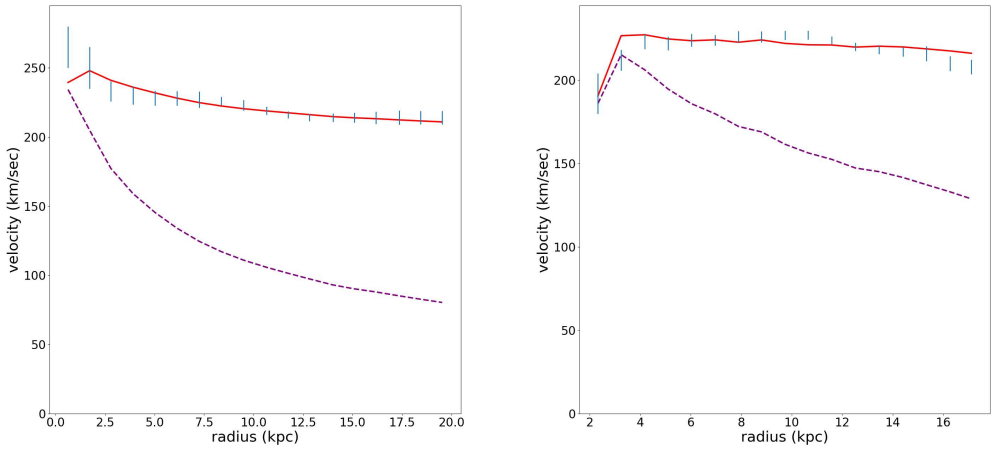

(**a**) (**b**)

Figure A2. *Cont.*

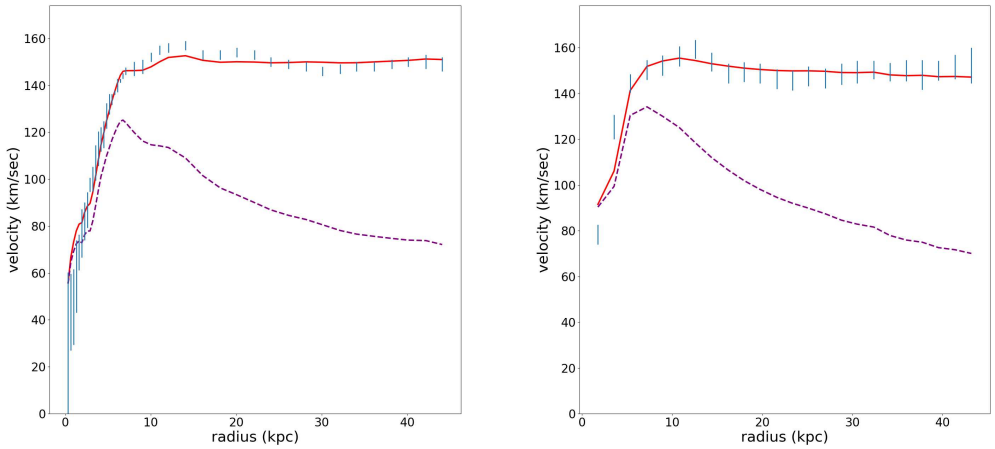

(**c**) (**d**)

Figure A2. Flat Rotation Curves. Lines are as in Figure A1 (**a**) NGC 7814 [29,84], (**b**) NGC 891 [29,84], (**c**) NGC 3198 [29], (**d**) NGC 3198 [57].

Appendix B.3. Ascending Rotation Curves

As can be seen in Figure A3, our model provides excellent fits to galaxies with ascending rotation curves—including examples of both gas dominated dwarf galaxies and intermediate spirals. Dwarf galaxies have been an important test case for dark matter models, giving rise to the cusp-core problem [85]. We present fit results here for two such galaxies. D 631-7, a dwarf irregular also known as UGC 4115, and IC 2574, a gas-dominated dwarf spiral galaxy, with no central stellar bulge. IC 2574 is problematic for dark matter model fits, as the model overestimates the inner RC out to 10 kpc [86].

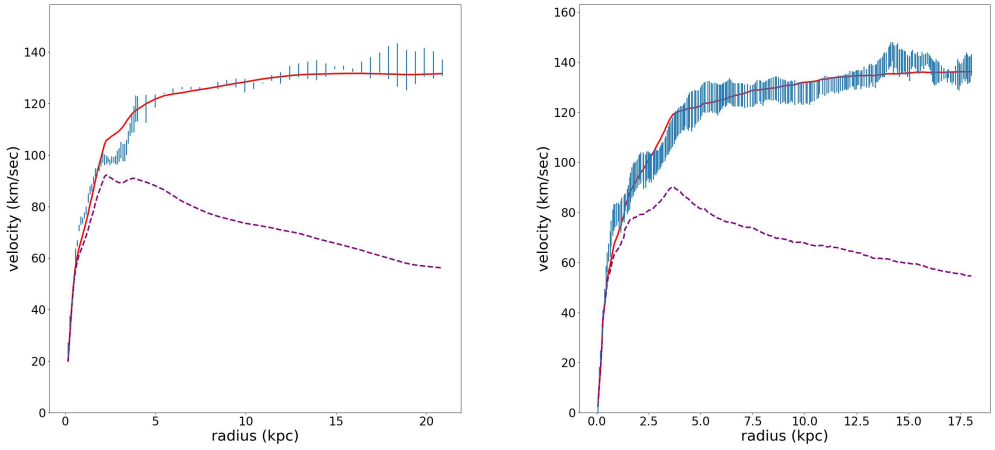

(**a**) (**b**)

Figure A3. *Cont.*

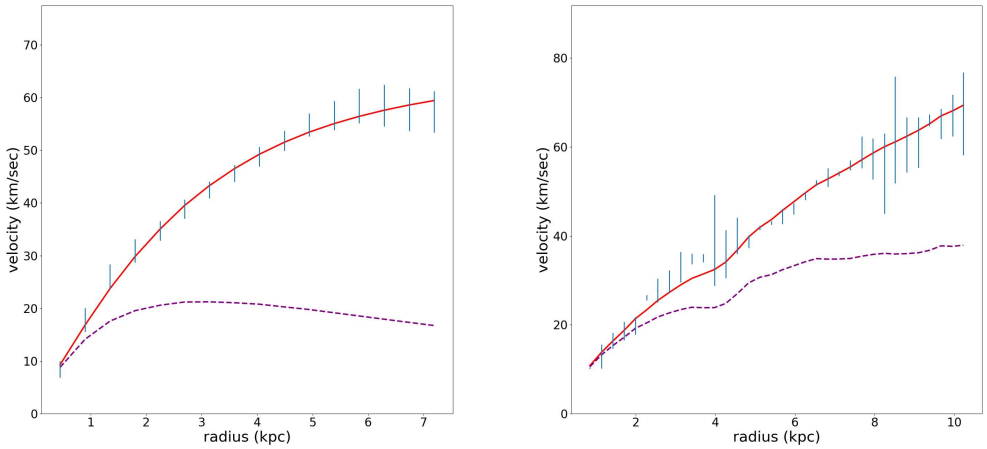

(**c**) (**d**)

Figure A3. Ascending Rotation Curves. Lines are as in Figure A1 (**a**) NGC 2403 [29], (**b**) NGC 2403 [56], (**c**) D 631-7 [29], (**d**) IC 2574 [29].

References

1. Rubin, V.C.; Ford, W.K., Jr. Rotation of the Andromeda Nebula from a Spectroscopic Survey of Emission Regions. *Astrophys. J.* **1970**, *159*, 379. [CrossRef]
2. Rubin, V.C.; Thonnard, N.; Ford, W.K., Jr. Extended rotation curves of high-luminosity spiral galaxies. IV—Systematic dynamical properties, SA through SC. *Astrophys. J.* **1978**, *225*, L107–L111. [CrossRef]
3. Bosma, A. The distribution and kinematics of neutral hydrogen in spiral galaxies of various morphological types. *Astron. J.* **1981**, *86*, 1791. [CrossRef]
4. van Albada, T.S.; Bahcall, J.N.; Begeman, K.; Sancisi, R. Distribution of dark matter in the spiral galaxy NGC 3198. *Astrophys. J.* **1985**, *295*, 305–313. [CrossRef]
5. Cebrián, S. Review on dark matter searches. *arXiv* **2022**, arXiv:2205.06833. [CrossRef]
6. Misiaszek, M.; Rossi, N. Direct Detection of Dark Matter: A Critical Review. *Symmetry* **2024**, *16*, 201. [CrossRef]
7. Akerib, D.S.; Cushman, P.B.; Dahl, C.E.; Ebadi, R.; Fan, A.; Gaitskell, R.J.; Galbiati, C.; Giovanetti, G.K.; Gelmini, G.B.; Grandi, L.; et al. Snowmass2021 Cosmic Frontier Dark Matter Direct Detection to the Neutrino Fog. *arXiv* **2022**, arXiv:2203.08084. [CrossRef]
8. Ostriker, J.P.; Peebles, P.J.E. A Numerical Study of the Stability of Flattened Galaxies: Or, can Cold Galaxies Survive? *Astrophys. J.* **1973**, *186*, 467–480. [CrossRef]
9. Rubin, V.; Ford, W.; Thonnard, N. Rotational properties of 21 SC galaxies with a large range of luminosities and radii. *Astrophys. J.* **1980**, *238*, 471. [CrossRef]
10. Persic, M.; Salucci, P. Dark and visible matter in Galaxies. *ASP Conf. Ser.* **1997**, *117*, 1.
11. Sofue, Y.; Rubin, V. Rotation Curves of Spiral Galaxies. *Annu. Rev. Astron. Astrophys.* **2001**, *39*, 137. [CrossRef]
12. McGaugh, S.S.; Schombert, J.M.; Bothun, G.D.; de Blok, W.J.G. The Baryonic Tully-Fisher Relation. *Astrophys. J.* **2000**, *533*, L99–L102. [CrossRef]
13. McGaugh, S. Galaxy Dynamics. *Conf. Proc.* **1999**, *182*.
14. McGaugh, S.S. The Mass Discrepancy-Acceleration Relation: Disk Mass and the Dark Matter Distribution. *Astrophys. J.* **2004**, *609*, 652–666. [CrossRef]
15. Tully, R.B.; Fisher, J.R. A new method of determining distances to galaxies. *Astron. Astrophys.* **1977**, *54*, 661–673.
16. Ziegler, B.L.; Böhm, A.; Fricke, K.J.; Jäger, K.; Nicklas, H.; Bender, R.; Drory, N.; Gabasch, A.; Saglia, R.P.; Seitz, S.; et al. The Evolution of the Tully-Fisher Relation of Spiral Galaxies. *Astrophys. J.* **2001**, *564*, L69. [CrossRef]
17. Persic, M.; Salucci, P.; Stel, F. The universal rotation curve of spiral galaxies—I. The dark matter connection. *Mon. Not. R. Astron. Soc.* **1996**, *281*, 27–47. [CrossRef]
18. Salucci, P.; Burkert, A. Dark Matter Scaling Relations. *Astrophys. J.* **2000**, *537*, L9–L12. [CrossRef]
19. Maschberger, T.; Bonnell, I.A.; Clarke, C.J.; Moraux, E. The relation between accretion rates and the initial mass function in hydrodynamical simulations of star formation. *Mon. Not. R. Astron. Soc.* **2014**, *439*, 234–246. [CrossRef]
20. Iocco, F.; Pato, M.; Bertone, G. Evidence for dark matter in the inner Milky Way. *Nat. Phys.* **2015**, *11*, 245–248. [CrossRef]

21. Li, P.; Lelli, F.; McGaugh, S.; Schombert, J. A Comprehensive Catalog of Dark Matter Halo Models for SPARC Galaxies. *Astrophys. J. Suppl. Ser.* **2020**, *247*, 31. [CrossRef]
22. Spinrad, H.; Taylor, B.J. The Stellar Content of the Nuclei of Nearby Galaxies. I. M31, M32, and M81. *Astrophys. J.* **1971**, *22*, 445. [CrossRef]
23. Conroy, C.; Gunn, J.; White, M. The Propagation of Uncertainties in stellar population synthesis modeling I: The relevance of uncertain aspects of stellar evolution and the IMF to the derived physical properties of galaxies. *Astrophys. J.* **2009**, *699*, 486. [CrossRef]
24. Munshi, F.; Governato, F.; Brooks, A.M.; Christensen, C.; Shen, S.; Loebman, S.; Moster, B.; Quinn, T.; Wadsley, J. Reproducing the Stellar Mass Halo Mass Relation in Simulated Lambda CDM Galaxies: Theory Versus Observational Estimates. *Astrophys. J.* **2013**, *766*, 56. [CrossRef]
25. Conroy, C. Modeling the Panchromatic Spectral Energy Distributions of Galaxies. *Annu. Rev. Astron. Astrophys.* **2013**, *51*, 393–455. [CrossRef]
26. Kurucz, R.L. Special Issue on the 10th International Colloquium on Atomic Spectra and Oscillator Strengths for Astrophysical and Laboratory Plasmas. *Can. J. Phys.* **2011**, *89*, 417–428. [CrossRef]
27. Levesque, E.M.; Leitherer, C.; Ekstrom, S.; Meynet, G.; Schaerer, D. The Effects of Stellar Rotation. I. Impact on the Ionizing Spectra and Integrated Properties of Stellar Populations. *Astrophys. J.* **2012**, *751*, 67. [CrossRef]
28. Yan, R.; Chen, Y.; Lazarz, D.; Bizyaev, D.; Maraston, C.; Stringfellow, G.S.; McCarthy, K.; Meneses-Goytia, S.; Law, D.R.; Thomas, D.; et al. SDSS-IV MaStar: A Large and Comprehensive Empirical Stellar Spectral Library—First Release. *Astrophys. J.* **2019**, *883*, 175. [CrossRef]
29. Lelli, F.; McGaugh, S.S.; Schombert, J.M. SPARC: Mass Models for 175 Disk Galaxies with Spitzer Photometry and Accurate Rotation Curves. *Astrophys. J.* **2016**, *152*, 157. [CrossRef]
30. Ciotti, L. On the Rotation Curve of Disk Galaxies in General Relativity. *Astrophys. J.* **2022**, *936*, 180. [CrossRef]
31. Hofmeister, A.M.; Criss, R.E. The physics of galactic spin. *Can. J. Phys.* **2017**, *95*, 156–166. [CrossRef]
32. Sipols, A.; Pavlovich, A. Dark Matter Dogma: A Study of 214 Galaxies. *Galaxies* **2020**, *8*, 36. [CrossRef]
33. Feng, J.Q. Rotating Disk Galaxies without Dark Matter Based on Scientific Reasoning. *Galaxies* **2020**, *8*, 9. [CrossRef]
34. Milgrom, M. A modification of the Newtonian dynamics—Implications for galaxies. *Astrophys. J.* **1983**, *270*, 371–389. [CrossRef]
35. Wald, R. *General Relativity*; University of Chicago Press: Chicago, IL, USA, 1984.
36. Tecchiolli, M. On the Mathematics of Coframe Formalism and Einstein and Cartan Theory. A Brief Review. *Universe* **2019**, *5*, 206. [CrossRef]
37. Jackson, J. *Classical Electrodynamics*, 3rd ed.; John Wiley & Sons, Inc.: Hoboken, NJ, USA, 1999.
38. Rindler, W. *Essential Relativity: Special, General, and Cosmological*; Springer: New York, NY, USA, 2013.
39. Casertano, S. Rotation curve of the edge-on spiral galaxy NGC 5907: Disc and halo masses. *Mon. Not. R. Astron. Soc.* **1983**, *203*, 735–747. [CrossRef]
40. Pomarède, D.; Tully, R.B.; Graziani, R.; Courtois, H.M.; Hoffman, Y.; Lezmy, J. Cosmicflows-3: The South Pole Wall. *Astrophys. J.* **2020**, *897*, 133. [CrossRef]
41. Schwarzschild, M. Mass distribution and mass-luminosity ratio in galaxies. *Astron. J.* **1954**, *59*, 273. [CrossRef]
42. Freeman, K.C. On the Disks of Spiral and S0 Galaxies. *Astrophys. J.* **1970**, *160*, 811. [CrossRef]
43. Binney, J.; Tremaine, S. *Galactic Dynamics*, 2nd ed.; Princeton University Press: Princeton, NJ, USA, 2008.
44. Bratek, Ł.; Jałocha, J.; Kutschera, M. On the axisymmetric thin disc model of flattened galaxies. *Mon. Not. R. Astron. Soc.* **2008**, *391*, 1373–1383. [CrossRef]
45. Bekenstein, J.D. Relativistic gravitation theory for the modified Newtonian dynamics paradigm. *Phys. Rev. D* **2004**, *70*, 083509. [CrossRef]
46. McGaugh, S.S. Milky Way Mass Models and MOND. *Astrophys. J.* **2008**, *683*, 137. [CrossRef]
47. Mistele, T.; McGaugh, S.; Hossenfelder, S. Galactic mass-to-light ratios with superfluid dark matter. *Cambridge* **2022**, *664*, A40. [CrossRef]
48. Loebman, S.R.; Ivezic', Z.; Quinn, T.R.; Bovy, J.; Christensen, C.R.; Jurić, M.; Roškar, R.; Brooks, A.M.; Governato, F. The Milky Way Tomography with Sloan Digital Sky Survey. V. Mapping the Dark Matter Halo. *Astrophys. J.* **2014**, *794*, 151. [CrossRef]
49. Huré, J.M.; Hersant, F. The Newtonian potential of thin disks. *Astron. Astrophys.* **2011**, *531*, A36. [CrossRef]
50. Chatterjee, T. Potential and force due to thin disk and spherical galaxies. *Astrophys. Space Sci.* **1987**, *139*, 243. [CrossRef]
51. de Vaucouleurs, G. Classification and Morphology of External Galaxies. *Handb. Phys.* **1959**, *53*, 275. [CrossRef]
52. McGaugh, S.S.; De Blok, W. Testing the hypothesis of modified dynamics with low surface brightness galaxies and other evidence. *Astrophys. J.* **1998**, *499*, 66. [CrossRef]
53. McGaugh, S.S.; Lelli, F.; Schombert, J.M. Radial Acceleration Relation in Rotationally Supported Galaxies. *Phys. Rev. Lett.* **2016**, *117*, 201101. [CrossRef]

54. Navarro, J. The Cosmological Significance of Disk Galaxy Rotation Curves. *arXiv* **1998**, arXiv:astro-ph/9807084. [CrossRef]
55. Bottema, R.; Pestana, J.; Rothberg, B.; Sanders, R. MOND rotation curves for spiral galaxies with Cepheid based distances. *Astron. Astrophys.* **2002**, *393*, 453. [CrossRef]
56. de Blok, W.; Walter, F.; Brinks, E. High-Resolution Rotation Curves and Galaxy Mass Models from THINGS. *Astron. J.* **2008**, *136*, 2648. [CrossRef]
57. Gentile, G.; Farnaey, B.; de Blok, W. THINGS about MOND. *Astron. Astrophys.* **2011**, *527*, A76. [CrossRef]
58. Xue, X.X.; Rix, H.W.; Zhao, G.; Re Fiorentin, P.; Naab, T.; Steinmetz, M.; van den Bosch, F.C.; Beers, T.C.; Lee, Y.S.; Bell, E.F.; et al. The Milky Way's Circular Velocity Curve to 60 kpc and an Estimate of the Dark Matter Halo Mass from Kinematics of 2400 SDSS Blue Horizontal Branch Stars. *Astrophys. J.* **2008**, *684*, 1143–1158. [CrossRef]
59. Sofue, Y. Mass Distribution and Rotation Curve in the Galaxy. In *Planets, Stars and Stellar Systems. Volume 5: Galactic Structure and Stellar Populations*; Oswalt, T.D., Gilmore, G., Eds.; Springer: Cham, Switzerland, 2013; p. 985.
60. Jiao, Y.; Hammer, F.; Wang, H.; Wang, J.; Amram, P.; Chemin, L.; Yang, Y. Detection of the Keplerian decline in the Milky Way rotation curve. *Astron. Astrophys.* **2023**, *678*, A208. [CrossRef]
61. McGaugh, S.S. The Imprint of Spiral Arms on the Galactic Rotation Curve. *Astrophys. J.* **2019**, *885*, 87. [CrossRef]
62. Lelli, F.; McGaugh, S.S.; Schombert, J.M.; Pawlowski, M.S. The Relation Between Stellar and Dynamical Surface Densities in the Central Regions of Disk Galaxies. *Astrophys. J.* **2016**, *827*, L19. [CrossRef]
63. McQuinn, K.B.W.; Boyer, M.; Skillman, E.D.; Dolphin, A.E. Using the Tip of the Red Giant Branch As a Distance Indicator in the Near Infrared. *Astrophys. J.* **2019**, *880*, 63. [CrossRef]
64. Kovács, G. Consistent distances from Baade–Wesselink analyses of Cepheids and RR Lyraes. *Mon. Not. R. Astron. Soc.* **2003**, *342*, L58–L62. [CrossRef]
65. Oh, S.H.; De Blok, W.; Walter, F.; Brinks, E.; Kennicutt, R.C. High-resolution dark matter density profiles of things dwarf galaxies: Correcting for noncircular motions. *Astron. J.* **2008**, *136*, 2761. [CrossRef]
66. Ivezić, Ž.; Kahn, S.M.; Tyson, J.A.; Abel, B.; Acosta, E.; Allsman, R.; Alonso, D.; AlSayyad, Y.; Anderson, S.F.; Andrew, J.; et al. LSST: From Science Drivers to Reference Design and Anticipated Data Products. *Astrophys. J.* **2019**, *873*, 111. [CrossRef]
67. McMillan, P.J.; Binney, J.J. Analysing surveys of our Galaxy ,Äì II. Determining the potential. *Mon. Not. R. Astron. Soc.* **2013**, *433*, 1411–1424. [CrossRef]
68. Fich, M.; Tremaine, S. The mass of the Galaxy. *Annu. Rev. Astron. Astrophys.* **1991**, *29*, 409–445. [CrossRef]
69. Koop, O.; Antoja, T.; Helmi, A.; Callingham, T.M.; Laporte, C.F.P. Assessing the robustness of the Galactic rotation curve inferred from the Jeans equations using Gaia DR3 and cosmological simulations. *Astron. Astrophys.* **2024**, *692*, A50. [CrossRef]
70. Sofue, Y.; Honma, M.; Omodaka, T. Unified Rotation Curve of the Galaxy—Decomposition into de Vaucouleurs Bulge, Disk, Dark Halo, and the 9-kpc Rotation Dip—. *Publ. Astron. Soc. Jpn.* **2009**, *61*, 227–236. [CrossRef]
71. Lin, H.N.; Li, X. The dark matter profiles in the Milky Way. *Mon. Not. R. Astron. Soc.* **2019**, *487*, 5679–5684. [CrossRef]
72. Crézé, M.; Chereul, E.; Bienaymé, O.; Pichon, C. The distribution of nearby stars in phase space mapped by Hipparcos: I. The potential well and local dynamical mass. *arXiv* **1997**, arXiv:astro-ph/9709022. [CrossRef]
73. Brownstein, J.R.; Moffat, J.W. Galaxy Rotation Curves without Nonbaryonic Dark Matter. *Astrophys. J.* **2006**, *636*, 721. [CrossRef]
74. Sanders, R.H. *The Dark Matter Problem: A Historical Perspective*; Cambridge University Press: Cambridge, UK, 2010.
75. Tully, R.B.; Courtois, H.; Hoffman, Y.; Pomarède, D. The Laniakea supercluster of galaxies. *Nature* **2014**, *513*, 71. [CrossRef]
76. Naidu, R.P.; Oesch, P.A.; van Dokkum, P.; Nelson, E.J.; Suess, K.A.; Brammer, G.; Whitaker, K.E.; Illingworth, G.; Bouwens, R.; Tacchella, S.; et al. Two Remarkably Luminous Galaxy Candidates at z [10–12] Revealed by JWST. *Astrophys. J.* **2022**, *940*, L14. [CrossRef]
77. Misner, C.W.; Thorne, K.S.; Wheeler, J.A. *Gravitation*; Princeton University Press: Princeton, NJ, USA, 1973.
78. Schombert, J.; McGaugh, S.; Lelli, F. The mass-to-light ratios and the star formation histories of disc galaxies. *Mon. Not. R. Astron. Soc.* **2018**, *483*, 1496–1512. [CrossRef]
79. Bell, E.F.; de Jong, R.S. Stellar Mass-to-Light Ratios and the Tully-Fisher Relation. *Astrophys. J.* **2001**, *550*, 212–229. [CrossRef]
80. Lelli, F.; McGaugh, S.S.; Schombert, J.M.; Pawlowski, M.S. One Law to Rule Them All: The Radial Acceleration Relation of Galaxies. *Astrophys. J.* **2017**, *836*, 152. [CrossRef]
81. Navarro, J.; Frenk, C.; White, S. The Structure of Cold Dark Matter Halos. *Astrophys. J.* **1997**, *462*, 563. [CrossRef]
82. Wiegart, T. Spiral Galaxy HI Models, Rotation Curves and Kinematic Classifications. Ph.D. Thesis, The University of Manitoba, Winnipeg, MB, Canada, 2010.
83. Battaglia, G.; Fraternali, F.; Oosterloo, T.; Sancisi, R. HI study of the warped spiral galaxy NGC 5055: A disk/dark matter halo offset? *Astron. Astrophys.* **2006**, *447*, 49. [CrossRef]
84. Fraternali, F.; Sancisi, R.; Kamphuis, P. A tale of two galaxies, light and mass NGC 891 and NGC 7814. *Astron. Astrophys.* **2011**. [CrossRef]

85. van den Bosch, F.C.; Swaters, R.A. Dwarf galaxy rotation curves and the core problem of dark matter haloes. *Mon. Not. R. Astron. Soc.* **2001**, *325*, 1017–1038. [CrossRef]
86. Navarro, J.F.; Benítez-Llambay, A.; Fattahi, A.; Frenk, C.S.; Ludlow, A.D.; Oman, K.A.; Schaller, M.; Theuns, T. The origin of the mass discrepancy-acceleration relation in ΛCDM. *Mon. Not. R. Astron. Soc.* **2017**, *471*, 1841–1848. [CrossRef]